IKONOS spatial resolution and image interpretability characterization

Robert Ryan[1*], Braxton Baldridge[2], Robert A. Schowengerdt[3], Taeyoung Choi [4], Dennis L. Helder [4], Slawomir Blonski [1]

[1]*Lockheed Martin Space Operations – Stennis Programs, Bldg. 1105, Stennis Space Center, MS 39529-6000 USA*

[2]*Booz Allen Hamilton, McLean, VA 22102-3838, now with Research Systems, Inc., Vienna, VA 22180 USA*

[3]*Department of Electrical and Computer Engineering, University of Arizona, Tucson, AZ 85721USA*

[4]*Department of Electrical Engineering, South Dakota State University, Brookings, SD 57007-0194 USA*

Abstract

This paper contains research results from five individual projects to characterize the spatial performance of the IKONOS commercial imaging sensor. The end result of the projects is determination of the spatial image quality of IKONOS data products in terms of the National Imagery Interpretability Rating Scale (NIIRS), the system Modulation Transfer Function (MTF), the system stability over the first year, the characteristics of the Space Imaging MTF Compensation (MTFC) procedure, and the application-specific capabilities of IKONOS imagery. Both panchromatic and multispectral imagery were evaluated. Major conclusions of this work are that the system was stable in imaging performance during the first year of operation, that its MTF meets the specification for the NASA Scientific Data Purchase program, that the initial MTFC processing appears to be transposed in the in-track and the cross-track directions, that the MTFC results in a

noise amplification of 2x to 4x in addition to sharpening the imagery, and that IKONOS panchromatic imagery achieves an average NIIRS rating of 4.5.

1. Introduction

The pre-eminent characteristic of IKONOS is its significantly higher spatial resolution compared to other non-military satellite remote sensing systems. Both the National Aeronautics and Space Administration (NASA) and the National Imagery and Mapping Agency (NIMA) have been purchasing IKONOS 1 m and 4 m ground sample distance (GSD) imagery for various purposes. NIMA acquires commercial satellite imagery as part of its mission to provide geospatial information to the Department of Defense (DoD) and to the national intelligence community. NIMA's vehicle for assessing the image quality and utility of commercial imagery is the Civil and Commercial Applications Project (CCAP). NASA Stennis Space Center purchases imagery primarily for land use research, and its academic partners at the University of Arizona and South Dakota State University are responsible for assessing image quality for NASA as part of the Scientific Data Purchase (SDP) Verification and Validation.

Although NASA and NIMA address significantly different sets of problems, both agencies are using this high-spatial-resolution imagery in similar ways. While the multispectral aspects of satellite systems have historically been exploited by NASA researchers, in the case of IKONOS, the 1 m panchromatic and pan-sharpened multispectral imagery have been used primarily for visual inspection and mapping applications, similar to the way such imagery is used by the defense communities (Garvin

et al., 2002; Tucker, 2002). NASA scientists rely upon the IKONOS spatial and geolocation characteristics primarily to detect and to identify small features .

The work presented here illustrates some of the complexities encountered when dealing with an emerging commercial product. While not commonly known, NASA negotiated its contract and data specifications with Space Imaging, LLC before the system was on-orbit and before all the present product options were available. NIMA negotiated its contracts with Space Imaging later resulting in different products being available to NASA and NIMA. One of the significant differences in offerings is that NIMA has the ability to purchase imagery that is radiometrically corrected without geometric correction, while NASA purchases only imagery that has been both radiometrically and geometrically corrected. The NIMA contract with Space Imaging calls the pure radiometric products "TIFF" and the resampled products "GeoTiff." At the time of the NASA contract negotiations, only cubic convolution resampling was available. NIMA contracted with Space Imaging to produce a nearest neighbor resampled product that later was made available to the NASA community.

Users of IKONOS imagery should investigate the relative benefits of each post processing option. The radiometry paper in this issue (Pagnutti et al., 2003) discusses the effects of Modulation Transfer Function Compensation (MTFC) on radiometry in various scene types. In this section, we focus on the spatial domain effects of the MTFC option. NASA was also initially offered imagery that had MTFC applied. MTFC is a form of image sharpening that attempts to correct the inherent Modulation Transfer Function (MTF) roll-off with spatial frequency caused by finite detector size, spacecraft motion,

diffraction, aberrations, atmospheric scattering, turbulence, and electronic effects (Holst, 1995).

One of the more interesting imaging product options has MTFC applied. Often, MTFC is used to boost the National Imagery Interpretability Rating Scale (NIIRS) rating and image interpretability. Applications that depend upon spectral analysis generally require higher Signal-to-Noise Ratio (SNR) than do purely visual applications. For both types of analyses, it is important to understand the effect of MTFC on SNR, as well as the spatial frequency content of the scene being studied, before selecting the MTFC processing option. In the sections below, we estimate the magnitude of effects produced by MTFC processing.

Another issue not generally known is that all the data are compressed, using a Kodak proprietary compression technique, off the focal plane from 11 bits/pixel to 2.6 bits/pixel for transmission to the ground. In the strict sense, this nonlinear compression violates the linear shift invariant requirement for MTF analysis. For these reasons, the results described in this paper should be interpreted as product-specific and are not the true fundamental engineering performance of the system. Product evaluations are becoming more common as we use additional commercial imagery sources and produce more complex products from government systems.

The intent of the spatial characterization effort funded by NASA–Stennis Space Center, under the Science Data Purchase program, and by NIMA is to:

- Evaluate the usefulness of IKONOS for image interpretation tasks
- Understand the types of spatial processing available from Space Imaging

- Evaluate the on-orbit spatial imaging performance of IKONOS
- Determine if any degradation has occurred during the first year of IKONOS operation

Research results that address these goals are presented in this paper. A variety of approaches are used including visual inspection, modeling, noise analysis, image gradients, and MTF. In Section I, we describe the relationships between image quality, edge response, and imagery options such as MTFC to the National Imagery Interpretability Rating Scale. NIIRS is a graduated, criteria-based, ten point scale used to indicate the amount of information that can be extracted by imagery (IRARS, 1996). In Section II, the University of Arizona describes relative image quality analysis using the image Digital Number (DN) gradient as a sharpness measure. In Section III, South Dakota State University (SDSU) describes MTF analysis using rectangular "pulse" targets. In Section IV, NASA describes MTF analysis using an "edge" target at the Stennis Space Center (SSC). In Section V, NIMA describes the application of IKONOS imagery in standard image interpretation tasks and NIIRS estimation with certified analysts.

Finally, we summarize the entire paper and tie together the various analyses and attempt to draw useful conclusions for future sensor characterizations.

2. Image quality in terms of NIIRS and edge response assessment estimates

The spatial resolution of most remote sensing systems is described in terms of the sensor MTF and GSD. In the case of IKONOS, the imagery NASA purchased was specified to have a GSD at nadir of 0.82 m in the panchromatic band and of 3.24 m in the multispectral bands. In addition, the minimum allowable MTF at the Nyquist frequency was specified to be 0.1 in the panchromatic band and 0.24 in the multispectral bands. These specifications, however, are for raw data and not for the products available to both NASA and NIMA.

Image quality is the result of a complex relationship between GSD, MTF, MTFC, and SNR. MTFC generally increases the sharpness and interpretability of the imagery, but it also introduces several artifacts, such as ringing at edges and increased noise. Visual interpretability ratings such as NIIRS can be estimated from the edge response, ringing overshoot, and SNR using the empirically based General Imagery Quality Equation (GIQE) (Leachtenauer et al., 1997). An edge response is determined from an image of extended bright and dark uniform rectangular areas of at least 10 x 20 pixels in extent or is estimated from a pulse or other target. The edge response is normalized such that the asymptotic dark and bright values are scaled to zero and unity, respectively. An important image quality metric used in the GIQE is the relative edge response (RER). The RER is the slope of a normalized edge, measured at ± 0.5 pixels from the edge center location. A commonly accepted form of the GIQE that accounts for the effects listed above follows:

$$NIIRS = 10.251 - a\log_{10} GSD_{GM} + b\log_{10} RER_{GM} - 0.656H_{GM} - \frac{0.344G}{SNR} \qquad (1)$$

Where GSD_{GM} is the geometric mean of the ground sampled distance, RER_{GM} is the geometric mean of the relative edge response, H_{GM} is the geometric mean-height overshoot caused by MTFC (Leachtenauer et al., 1997), and G is the noise gain associated with MTFC. In the current form of the GIQE, SNR is estimated for differential radiance levels from Lambertian scenes with reflectances of 7 percent and 15 percent with the noise estimated from photon, detector, and uniformity noise terms. If the RER exceeds 0.9, then *a* equals 3.32 and *b* equals 1.559; otherwise, *a* equals 3.16 and *b* equals 2.817.

The GSD is computed in both ground plane directions in inches, from which GSD_{GM} is then calculated. Similarly, the RER_{GM} is the geometric mean of the RERs computed in the orthogonal image directions. The GIQE overshoot H accounts for the ringing associated with the MTFC and is measured over 1.0 to 3.0 pixels from the edge in 0.25-pixel increments. In most cases, the overshoot H is the maximum value over this range. However, if the response is monotonic over this range, the overshoot H is taken as the value at 1.25 pixels from the edge. Again, H is estimated in orthogonal image directions and the geometric mean is calculated. The noise gain term is defined in Equation 2:

$$G = \left[\sum_{i=1}^{N} \sum_{j=1}^{N} \left(MTFCkernel_{ij} \right)^2 \right]^{\frac{1}{2}} \tag{2}$$

Noise gain associated with the MTFC processing was investigated using simulated scenes with the expected noise properties of IKONOS imagery and estimating the root sum square of the MTFC kernel provided by Space Imaging. Table 1 lists the estimated noise gain associated with each band. The panchromatic noise gain is approximately 4,

being twice that of the multispectral bands with the multispectral band noise increasing with wavelength. The simulation results and expression (2) are in good agreement. Although Space Imaging implements its MTFC option in the spatial domain, the MTFC is described here in the frequency domain as provided by Space Imaging to NASA for analysis. MTFC functions are designed to boost the higher spatial frequencies without impacting the zero spatial frequency. The IKONOS panchromatic MTFC function is a monotonic function increasing from unity at zero spatial frequency to over 6 at the Nyquist frequency. This function is calculated by zero-padding a fast Fourier transform of the MTFC kernel. The function is a relatively symmetrical flower petal shape, but it is slightly stronger in the cross-track direction than in the in-track direction. Although not shown here, NASA also derived the MTFC by estimating the transfer function from several georeferenced scenes, with and without MTFC. The magnitude and shape of the MTFC functions qualitatively agreed with the functions provided by Space Imaging, but NASA found that the transfer functions were always rotated from true north by several degrees or more because Space Imaging used a kernel that combines the resampling and MTFC processing.

2.1 MTFC simulated edge effects

Simulated edge responses were generated assuming a symmetrical Gaussian MTF with an MTF at the Nyquist frequency of 0.1, the IKONOS MTF specification for panchromatic imagery. A Gaussian MTF function was chosen because many system MTF functions are approximately Gaussian in shape. NASA did not consider any resampling in these simulations. The expected asymmetries were ignored because NASA

lacked sufficient system information to model them accurately. The simulations are thus approximations, but they do illustrate several features seen in other sections of this paper. The simulations start with an 8x oversampled edge response that is then decimated to the supplied sampling. In the case of panchromatic imagery, a simulated edge is generated at a 0.108 m GSD for the simulations and then resampled to 0.82 meters to allow examination of the effects of sampling and aliasing on the edge response. A second set of edge responses was generated by applying the MTFC processing. In the real imaging process, the individual detectors sample a continuous function with the relative sampling controlled by the focal length, slant range, and detector spacing, while the absolute position relative to an edge is a random process. This level of oversampling minimizes any aliasing effects in the simulation. The magnitude of the ringing depends on the phasing of the sampling. The overshoot was about 10 percent and the RER improved by approximately 50 percent.

The multispectral MTFC functions are not as strong as the panchromatic MTFC; their peak values are less than one half the panchromatic MTFC peak. This is not surprising since the IKONOS multispectral specification for MTF at the Nyquist frequency is 0.24. Also, the MTFC functions are stronger as wavelength increases. The overshoot is under a few percent for all bands. Each MTFC function should be different for each multispectral band, since both diffraction and charge coupled device MTF functions are wavelength dependent. The multispectral MTFs are also far more asymmetric than the panchromatic MTFC function. The near-infrared (NIR) MTFC function is the most symmetric and the blue band is the most asymmetric, with each MTFC function being stronger in the cross-track direction than in the in-track direction as seen in the blue band edge response

simulations. This calculation is similar to panchromatic calculations but with the multispectral MTF at the Nyquist frequency set to 0.24 for the simulations. The MTFC processed edge showed only minimal change in the in-track direction. Because the MTF typically rolls off more quickly in the in-track direction, the MTFC was expected to be stronger in the in-track direction. At the time of this writing, NASA and Space Imaging had discussed this finding, and Space Imaging is considering rotating the kernels.

3. Multispectral and panchromatic band relative image analysis

3.1 Introduction

Constructed and cultural targets can be used for MTF analysis of satellite imaging sensors (Schowengerdt et al., 1985; Rauchmiller and Schowengerdt, 1988; Storey, 2001). Examples of target use for MTF analysis of IKONOS are included in the SDSU and SSC sections of this paper. However, logistical difficulties with constructed targets and lack of control of cultural targets, such as bridges, roads, and other linear features, make target-free approaches to image-quality evaluation desirable. This section describes such an approach undertaken from July 2000 to July 2001 to determine IKONOS image quality stability.

3.2 Rationale

Two images of the same area taken at different times will have unique characterizations due to changes in surface cover, solar illumination angles, sensor view angles, atmospheric conditions, and sensor performance. If the non-sensor-related factors

are negligible for a given pair of images, then it would be possible to use the image pair for an evaluation of change in sensor performance. The DN gradient (i.e., the discrete derivative between neighboring pixels) is proposed as an image quality metric. It is well known that the DN gradient is directly related to the "sharpness" of an image. The image pair to be compared is first processed to extract the same ground region and to match the DN histograms on a global basis (Schowengerdt, 1997). The latter step removes global (consistent over the whole image) solar irradiance variations due to different solar angles and global atmospheric transmittance or path radiance differences on the two dates.

The DN gradient calculation, we chose the Roberts gradient, the magnitude of the vector sum of neighboring pixel differences in the ±45° directions, which is a long established way to obtain an image gradient (Castleman, 1996).

3.3 Sensitivity

Two examples will be used as reference benchmarks for this image comparison technique. Both are panchromatic images processed without MTFC and with MTFC. One image is of the Big Spring, Texas, MTF target maintained by Space Imaging for IKONOS evaluation, and the other image is of Tucson, Arizona. The differences are visually substantial in both cases as shown in Figure 1. The target image represents a relatively simple scene consisting almost entirely of edges and lines. The Tucson image is a more complex scene consisting of cultural features similar to those in the anniversary image with which it was compared (the only difference was some offset due to different frame locations). Because the image collects are the same in both cases, there are no differences other than those caused by MTFC. Comparison of the average gradient

yielded the results in Table 2. Therefore, average DN gradient differences on the order of 30 to 45 percent are expected in comparison of MTFC-on and MTFC-off processed images.

3.4 Image quality stability

Two IKONOS collects were obtained over Tucson, Arizona, on July 23, 2000, and on July 15, 2001. The solar and sensor angles for these collects are given in Table 3. Solar azimuth and elevation affect the length and direction of shadows and affect the overall irradiance of level terrain by the cosine of the solar zenith angle (Schowengerdt, 1997). The effect of sensor azimuth and elevation on the recorded image is more complex. For example, in the case of high-resolution sensors such as IKONOS, sensor azimuth and elevation can determine whether one side of building is seen. In addition, specular reflection can occur from small, directional objects, such as vehicle windshields and metal roofs. In this case (Table 3), the cosine irradiance factor between the collects in 2000 and 2001 is 1.0348, or only about 3 percent. This factor was applied as a gain to the 2000 image to normalize it to the same average irradiance as the 2001 image.

Two areas were extracted from each year's image and the Roberts gradient was applied to each area. The areas were chosen to avoid significant land cover changes (e.g., new pavement on a parking lot or road) and were registered visually when cut from the images. One of the characteristics of this technique for image comparison is that it is not particularly sensitive to image misregistration of a few pixels. Since a large area is used, the average gradient magnitude is little affected by a slight offset in either image. The average DN gradient magnitudes calculated from the image regions are given in Table 4.

The average percentage difference on the two dates was 4.6 percent for Area 1 and 8.9 percent for Area 2. In both cases, these differences are much less than the nearly 50 percent difference between the MTFC-off and MTFC-on images for the Big Spring target and Tucson data (Table 2).

3.4 Summary and conclusions

A simple relative-analysis technique for measuring sharpness was applied to two IKONOS collects of Tucson, Arizona, taken approximately a year apart. Using the average gradient magnitude as a measure of image sharpness, the two images differ by less than 10 percent. Relative to the gradient magnitude difference of 30 to 45 percent between images with and without MTFC, the two images acquired approximately a year apart have the same image quality. Other than imaging system performance changes, factors that could cause the 10 percent difference include differences in sensor look angles, changes in land cover, and differences in solar irradiance angles. These factors were minimized in this study by using images with high sensor elevation angle, by selecting image regions with little land cover change, and by using image collects with solar elevation and azimuth angles within 5° of each other.

4. On-orbit MTF measurement by SDSU

4.1 Introduction

This section describes a procedure that was developed for estimating the Edge Spread Function (ESF) and MTF of high spatial resolution imaging sensors while in orbit. No

underlying mathematical model is assumed since complete system descriptions for typical sensors are rarely available.

4.2 Method description

The primary target consisted of a set of 3 m x 30 m blue tarps placed in a relatively uniform grassy field and oriented in a 2 x 4 pattern representing a rectangular shape 12 m x 60 m in size. The 60 m length extended from north to south as shown in Figure 2. As shown in the figure, these tarps are quite bright in the blue with approximately 0.4 for reflectance. As wavelength increases, the reflectivity decreases until reflectances in the red wavelengths are nearly the same as vegetation. However, in the NIR, reflectance again increases to nearly 0.4. Thus, this target is particularly well suited for MTF evaluation of multispectral imagery in the blue and in the near infrared.

Tarp 1 and tarp 2 (T1 and T2) were selected as reference tarps. They were aligned by surveyor's transit at an angle of 8° east of true north to obtain as straight an edge line as possible. In addition, all seams were aligned by transit to maintain straight edges. To understand better the importance of target angle, an example ESF is shown in Figure 3. All pixel centers are shown as dotted angled grids. The dashed lines indicate the phasing of the pixel center locations as the edge location changes with each row of pixels. The horizontal axis is scaled in units of pixels corresponding to one ground sample interval in the output image. The vertical axis, in units of digital number, represents the value of each pixel. The output edge function is then sampled at a resolution of 20 points per pixel. As the orientation of the angle changes, the resolution changes as well, becoming either coarser or finer. Optimal angles exist that place the subpixel sample locations on a

uniform grid with the limited target length. Because IKONOS imagery is resampled so that true north is "up," an optimal target angle for both panchromatic and multispectral bands was found to be 8° east of true north.

This method's first step involves determining exact edge location. Edge positions are determined on a line-by-line basis using available pixel information. For example, a blurred edge is shown in Figure 4. Simple digital differentiation has been applied to detect maximum slope. The subpixel edge points are determined by fitting a cubic polynomial to the edge data using four values around the maximum slope point. The zero crossing location of the second derivative indicates the curve's inflection point, which is then assumed to be the subpixel edge location.

An underlying assumption is that the edge of the target lies in a straight line. Any deviations from a straight edge represent errors in the geometry of the image and a potential contribution to the overall MTF of the system. With this thought in mind, all edge cross-sections were forced to lie along a straight line by fitting a least squares line through the subpixel edge locations obtained from the previous step and then declaring that the actual edge locations lie on that line. In Figure 5, the circles on the edge show the input edge positions for individual rows of pixels. The line represents the least squares estimate for all edge positions. Cubic splines were then used to interpolate each usable horizontal row of "aligned" edge data. Twenty values were interpolated within one pixel point to build a pseudo-continuous line. All vertical rows were used to estimate one averaged spline as shown in Figure 6.

The tarp width should be carefully chosen because of the zero crossing points in the sinc function. This is especially important since many imaging systems are required to

meet minimum specifications of MTF at the Nyquist frequency. A tarp width of one pixel does not include any zero crossing points before the Nyquist frequency; however, the output signal from such an input is too small and may likely be affected by noise. With tarp widths of two, four, or six pixels, the Nyquist frequency occurs at the zero crossing point; when the output FT is divided by the input FT, the MTF value at the Nyquist frequency cannot be determined. To compute MTF values at the Nyquist frequency, a tarp width of three pixels appears to be optimal. Although a three-pixel wide input contains one zero crossing point between zero and the Nyquist frequency, the width is large enough to produce a well-defined image target and the output signal is strong enough to be minimally affected by noise.

4.3 Results

As shown in Figure 7, the width of the pulse was determined by the actual tarp width. Edge detection was applied on every row, and the subpixel edge positions were adjusted by the least squares fitting line. The average profile was normalized by the difference between the mean grass DN value and the mean tarp DN value. The input pulse and the adjusted output were then Fourier transformed (Figure 8); the curve denoted with stars is the discrete Fourier transform of the output and the plot with circles is the Fourier transform of the input pulse. Finally, the MTF was calculated by dividing each output value by its corresponding input and by normalizing the result by the spatial average component magnitude. The resulting MTF, shown in Figure 9, has a value at the Nyquist frequency of approximately 0.31.

One of the drawbacks of working with pulse type targets is that in Fourier space, the corresponding function is a sinc function that has a number of zero crossings. In a noiseless system, the output response would also be zero at these frequencies. However, because noise is always present in real systems, significant errors will often be introduced at frequencies near where these zero crossings occur. Because the input function is rapidly approaching zero near the zero crossing frequency, division in Fourier space will often produce noticeable errors in MTF at frequencies close to where the zero crossings occur. An apparent anomaly observable in Figure 11 at the normalized frequency 0.3 where the MTF function value is larger than what the overall MTF curve suggests it should be.

Figures 10 and 11 exhibit all four pulse spread functions and MTFs obtained during the summer 2001 season. Figure 10 shows a consistent estimate of the pulse spread function with undershoot visible on each side of the pulse. Figure 11 shows good repeatability of MTF estimation with the single exception noted above. Estimates near the input sinc function zero crossing frequency (i.e., between f=0.3 and f=0.4) show more variability.

4.4 Summary

This work was an attempt to characterize the performance of a high-spatial-resolution imaging system in orbit by estimating its frequency response to ground inputs. The tarp-based target provided a usable pulse input for the four-meter multispectral bands. The physical layout of the target was found to be critical for a reasonable MTF estimation; proper orientation of the target enabled reasonable determination of subpixel edge

locations. The MTF results obtained from IKONOS images suggested that the minimum value at the Nyquist frequency for the multispectral bands was 0.27, exceeding NASA's Scientific Data Purchase specifications.

5. MTF analysis using the Stennis Space Center target

5.1 Introduction

Spatial resolution of image products is affected not only by characteristics of the satellite camera but also by processing of the images after reception at a ground station. Image processing may include such steps as geometric correction and geographic registration as well as image sharpening based on MTF compensation. Because the spatial resolution characterization is conducted for the on-orbit satellite, the imaging process is also affected by transmission of radiation through the Earth's atmosphere. Therefore, characterization of the spatial resolution of image products involves evaluation of the entire remote sensing system.

Full width at half maximum of a line-spread function is used as a measure of spatial resolution of the images. Before LSFs are derived from edge responses by numerical differentiation, the edge responses are measured and analyzed using a modified knife-edge technique (Tzannes and Mooney, 1995). Adjacent black and white square panels, either painted on a flat surface or deployed as tarps, form a ground-based edge target used in the tests. During the measurements, the edge target is intentionally oriented so the image of the edge is aligned slightly off-perpendicular to a pixel grid direction. The tilted-edge modification to the original knife-edge method allows properly sampled edges

to be obtained, minimizing aliasing (Reichenbach et al., 1991). To measure an edge response, a rectangular region containing the tilted edge is extracted from an image of the edge target as shown in Figure 12. In such a region, each line across the edge forms an approximate edge response. Exact edge responses (in the direction perpendicular to the edge) are obtained when distances are additionally scaled by cosine of the tilt angle. The distance correction is usually small, but it becomes important when results from measurements with different edge orientations are to be compared.

Size of the edge target panels is a critical factor in spatial resolution measurements of satellite images. To accommodate the 1-meter GSD of the IKONOS panchromatic images, panels 20 m by 20 m in size are used. Larger panels would provide even more accurate measurements, but deployment of such large targets becomes extremely difficult. Therefore, the number of edge response samples available for analysis is still limited by the target size even with the additional sampling provided by the edge tilt. For panels of given size, sampling of the spatial response is also affected by the edge tilt angle. When deployable tarps are used in the measurement, orientation of the edge can be optimized for maximum oversampling. Based on pre-test simulations, a tilt angle of 5° was selected and used in measurements conducted with a set of specially coated, reflective tarps owned and operated by the NASA Earth Science Applications Directorate at Stennis Space Center.

With a limited number of the available edge response samples, image noise may significantly affect the results of a spatial resolution characterization. Not only does numerical differentiation of an edge response amplify the noise present in the data and produce a spurious LSF, but also determination of the edge response slope becomes less

accurate. To mitigate adverse effects of image noise and limited sampling, a smooth, analytical function is fitted to the edge responses. In the present approach, a superposition of three sigmoidal functions is utilized. Only three functions are used because too many components could cause the analytical function to fit the data points too well and to reproduce the noise and errors rather than the actual information. Thus, the fitting is performed for all the edge responses simultaneously using the formula in Equation 3:

$$e_i(x) = d + \sum_{k=1}^{3} \frac{a_k}{1 + \exp\left|\frac{x - b_1 \Delta i - b_2}{c_k}\right|} \tag{3}$$

The distance x is measured in the direction perpendicular to the edge. The nonlinear least-squares optimization is conducted for nine parameters: a_1, a_2, a_3, c_1, c_2, c_3, b_1, b_2, and d. Expanding on the work of Tzannes and Mooney, position and orientation of the edge are found simultaneously with the parameters characterizing spatial resolution: in one computational process of a nonlinear least-square fit of the two-dimensional analytical function to the intensities in the edge image. The parameters a_k, b_1, b_2, and c_k are common for all the edge responses, while the difference in the edge position is introduced by the edge response index (i) multiplied by image GSD (Δ). Because all of the edge positions are located on a straight line, they are specified with the simple formula $b_1 \Delta i + b_2$. Tangent of the tilt angle is equal to the absolute value of the parameter b_1. To further suppress noise artifacts, all three sigmoidal functions are restricted to the same positions of the edge specified by the parameters b_1 and b_2. This assumption also ensures that the analytical edge response function is symmetrical.

Examples of the measured edge responses and the analytical functions fitted to them are shown in Figure 13. The presented analyses were conducted for IKONOS panchromatic image products that were georeferenced using the cubic convolution resampling and the Universal Transverse Mercator projection with the WGS-84 datum. The satellite acquired two source images on different dates: one for measurement of the edge response in the easting direction (along the rows of image pixels) and the other for measurement of the edge response in the northing direction (along the columns of the image pixels). Each of the source images was used to create two different image products by processing it either with MTFC-on or MTFC-off. In this way, effects of MTFC on spatial resolution of the images can be directly evaluated by studying this set of four images. Finding the parameters b_1 and b_2 during the curve-fitting process is equivalent to shifting the edge responses to a single reference location so that all the edge points are aligned. Superimposing all the shifted edge responses creates a new one with a finer spatial sampling as shown in Figure 14. Comparison of the measured edge responses with the fitted, analytical functions indicates that the edge responses are asymmetric. The asymmetry is noticeable even in the images processed without the MTF compensation. For the images with MTFC, the measured edge responses additionally contain apparent overshoots and undershoots. The analytical function does not fit those secondary features exactly, but it does reflect the general shape of the measured edge response. Nevertheless, it is evident that the MTFC greatly improves spatial resolution of the IKONOS images and makes the edge responses much steeper.

After an analytical edge response function is obtained from the best fit, it is differentiated numerically to derive LSF and its FWHM as shown in Figure 15. The edge

responses were extracted five times from each of the images by independent selection of the analysis area. Mean results of the FWHM measurements obtained by averaging the five samples are listed in Table 5. To characterize spatial resolution of the IKONOS panchromatic images, the FWHMs should be compared with the 1 m GSD of the resampled image products. Such comparison shows once again that the MTFC clearly increases sharpness of the IKONOS images. In absolute terms, both images acquired in the early months of 2002 have rather narrow LSFs even without the MTFC applied. These results confirm high spatial resolution of the IKONOS panchromatic images.

6. Assessing imagery utility for NIMA: IKONOS panchromatic image interpretability study

6.1 Introduction

The NIMA Civil and Commercial Applications Project performed an interpretability study of IKONOS-2 panchromatic imagery to evaluate the information content of IKONOS imagery in support of standard image interpretation tasks supporting military and civilian applications. The metrics used to gauge utility in this study were the NIIRS and task satisfaction of Essential Elements of Information (EEI). An EEI represents a request for intelligence information. The EEIs were restated in terms of image observables and related tasks. For example, an EEI might ask the intelligence analyst to determine the number of long-range tactical aircraft. The observable might be large camouflaged fighter aircraft. The task is "detect large camouflaged fighter aircraft." Image task EEIs are associated with a Visible NIIRS level; e.g., a NIIRS 3 image would

be able to satisfy all level 3 EEIs. EEIs are derived from a variety of sources, such as NIIRS criteria and the NIMA Community Needs Forecast. The EEIs chosen for the IKONOS panchromatic evaluation addressed image tasks for NIIRS levels 3 through 6.

6.2 Methods

Twenty-four level 1 TIFF panchromatic images were acquired from Space Imaging. TIFF products are radiometrically corrected only. Sensor arrays are joined and contrast balanced; geometric distortions are not eliminated, and the GSD for each pixel increases with distance from nadir (mean collected GSD of 0.97 m for level 1 imagery). Fifteen archived IKONOS level 2 GeoTIFF panchromatic images were acquired from the DoD's Commercial Satellite Imagery Library. GeoTIFF image products have been radiometrically and geometrically corrected and resampled to the Universal Transverse Mercator projection, hence each pixel has been resampled to a uniform 1-meter GSD (mean collected GSD of 0.99 m for level 2 imagery). Imagery collection dates ranged from November 1999 to July 2000.

The image matrix used in this evaluation was intended to provide scene coverage of tropical, arid, northern temperate, and southern temperate climate regimes within a single season. Images were examined for Order of Battle content, and image subsets were selected or "chipped" out. A total of 72 image chips were used in the evaluation: 46 image chips were created from the 24 TIFF images, and 26 image chips were created from the 15 GeoTIFF images. A chipping routine was used to generate the image chips and a two-power (2x) enlargement. The 2x version was created for each chip using nearest-neighbor resampling and applying an identical histogram stretch as the 1x

version. Each chip pair (1x and 2x) was rotated to the appropriate cardinal direction that best aligned image obliquity to the top of the display.

The evaluation was conducted at the NIMA Imagery Support and Assessment Branch's softcopy evaluation facility. All evaluation participants used the same workstation with a precision color monitor, which was calibrated before the start of the evaluation. The monitors were set to a minimum luminance response of 0.10 fL and a maximum luminance response of 35.0 fL. Evaluation participants were free to roam and zoom at 1x or 2x magnification within the image. All ratings were made at 2x. No interactive enhancement of the imagery was allowed, and image chips were rendered with no additional processing.

Participants for this evaluation consisted of eight NIMA Visible NIIRS-certified imagery analysts. Evaluation participants were experienced with assessing OB as well as natural and cultural features on panchromatic imagery. The evaluation procedure consisted of each participant's reviewing a sequence of panchromatic (pan) scenes on the softcopy workstation and responding with both NIIRS ratings and task satisfaction confidence ratings for each scene. Examples of specific questions used are as follows:

- Determine the NIIRS rating for this image
- What is your confidence in your ability to identify areas suitable for use as light fixed-wing aircraft (e.g., Cessna, Piper Cub, Beechcraft) landing strips?

NIIRS ratings and EEI responses were given for each panchromatic scene before advancing to the next scene. The Visible NIIRS manual was available for reference during the evaluation. The task satisfaction scores are given on a 0–100 confidence rating

scale, where 0 means the task cannot be performed and 100 means the task is certain to be performed. The analysts were instructed to assume that normal collateral imagery and information about the target were available. All ratings and responses were entered by way of a graphical user interface sliding bar.

6.3 Results

Eight imagery analysts completed the evaluation over an 11-day period. The final dataset consisted of 72 NIIRS ratings and 250 confidence ratings of the EEI tasks for 72 image chips. Statistical analysis of the data began with the standard assessment of reliability and consistency. The inter-rater correlation, rater-group correlation, and Cronbach's alpha were computed to examine consistency and reliability among the imagery analysts. The rater-group correlations ranged from .68 to .75 and the alpha was .89, indicating a high degree of consistency among the raters. Analysis of Variance was used to identify outliers in the datasets. One image was removed from the NIIRS dataset and two images were removed from the EEI confidence ratings. These cleaned datasets were used for all further analyses. The average NIIRS value for TIFF pan images was 4.65 based on a population of 46 image chips obtained from 24 image products. The average NIIRS value for GeoTIFF pan images was 4.41 based on a population of 26 chip sets from 15 image products.

For these levels of NIIRS for the TIFF imagery, the RER is approximately 0.7. Approximately a 0.4 NIIRS improvement is expected with MTFC processing based on the GIQE.

6.4 NIIRS ratings

The first step in obtaining NIIRS ratings was to calculate descriptive statistics. Then an ANOVA was conducted to examine the difference in ratings for format (GeoTIFF vs. TIFF) and climate (Arid, Tropical, Temp (N), Temp (S)), including GSD as a covariate. For all analyses that include GSD, the collected GSD was used (as opposed to the resampled GSD) and was transformed to $\log_{10}$. Climate was not found to be significantly different, so the variable was dropped from further analyses. An Analysis of Covariance was conducted to determine the impact of format on mean NIIRS. The analysis included $\log_{10}$GSD as a covariate, as well as an interaction term between $\log_{10}$GSD and format. The analysis revealed that format was not a significant main effect, but $\log_{10}$GSD ($p = .02$) and the interaction term ($p = .07$) were significant predictors of NIIRS ($R^2 = .19$). These results indicate that format does not directly impact NIIRS ratings. The 0.24 difference in mean NIIRS between TIFF and GeoTIFF is based on the average differences in GSD and the interaction between GSD and format. TIFF imagery has a lower average GSD (.931 meters) than GeoTIFF (.993 meters), thus accounting for higher NIIRS ratings. These results were used to derive simplified regression Image Quality Equations, predicting NIIRS from $\log_{10}$GSD for both formats:

$$GeoTIFF\ predicted\ NIIRS = 4.41 - 0.77 \cdot \log_{10} GSD \quad (4)$$

$$TIFF\ predicted\ NIIRS = 4.52 - 5.05 \cdot \log_{10} GSD \quad (5)$$

However, because of the limited range of GSD (0.8 to 1.3 meters), it was not possible to fit an IQE to predict NIIRS with great accuracy. The predicted NIIRS was the same for both formats at a GSD of 1.06 meters. It is useful to compare equations (1) and (2) to the

GIQE derived to predict NIIRS based on electro-optical parameters and system design (General Image Quality Equation (GIQE) User's Guide, 1996). The slope for the TIFF equation is much steeper than the GIQE-obtained -3.32; however, a 95 percent confidence interval includes -3.32, indicating that GSD is a significant predictor of NIIRS ratings for TIFF imagery. On the other hand, the confidence interval for GeoTIFF regression slope includes zero, indicating that GSD may not be a significant predictor of NIIRS for GeoTIFF imagery.

If the slope were indeed zero, then the NIIRS value for this imagery does not depend on the collected GSD. Since GeoTIFF images have been resampled to have a processed GSD of one meter regardless of collected GSD, a slope of zero is not unreasonable. However, the zero slope can be true only over a very limited range of GSD. For example, an image with a collected GSD of two meters that has been resampled to one meter clearly will not be as good as an image with a true GSD of one meter. Thus it is hypothesized that over a larger range of GSD, equation (4) would be a broken line with two slopes instead of a straight line, with the break occurring at or near one meter. The slope for GSD less than one meter would be zero or possibly somewhat negative. The slope of GSD greater than one meter would be comparable to EO panchromatic imagery characterized by the GIQE; i.e., about -3.31.

6.5 Essential elements of information

Means and standard deviations were calculated for the 250 confidence ratings for various EEIs. Each EEI had an associated NIIRS level obtained from a previous evaluation. ANCOVAs were conducted to compare confidence ratings by climate, NIIRS

level, and format, including $\log_{10}$GSD as a covariate. NIIRS levels were determined by rounding the NIIRS requirement for each task to the lower level (i.e., a 3.2 and a 3.8 rating would both be NIIRS Level 3). Mean EEI confidence ratings were analyzed by climate, format, $\log_{10}$GSD, and NIIRS level and their interactions. Format, level, and $\log_{10}$GSD were found to be significant ($R^2 = .476$, $p < .04$). Unlike the NIIRS ratings, the interaction between $\log_{10}$GSD and format was not significant. Next, the main effects for the two categorical variables were explored. TIFF had an average of 6.3 points higher than GeoTIFF, indicating that raters had more confidence in their ratings for TIFF images.

A Tukey post hoc test was conducted to determine which NIIRS levels differed significantly from one another. The test indicated that all paired comparisons were significantly different ($R^2 = .45$, $p < .01$). Because NIIRS level 3 EEIs are the easiest to answer, they had the highest mean EEI confidence ratings, while level 6 EEIs had the lowest mean confidence ratings. A confidence rating of 75 percent indicates that the task can be satisfied with reasonable confidence. The results indicated that GSD and the interaction of the GSD*format term was significant in predicted NIIRS ratings. Thus, the .24 mean NIIRS difference between TIFF and GeoTIFF was due to the lower average GSD for TIFF imagery. The analyses of the EEI confidence ratings showed two main effects for format and NIIRS level. TIFF imagery had higher mean EEI ratings than did GeoTIFF imagery. Also, level 3 NIIRS had the highest EEI ratings (indicating the most confidence) while level 6 NIIRS had the lowest EEI ratings (indicating the least confidence).

6.6 Conclusion

An average NIIRS rating of 4.5 was achieved with IKONOS pan imagery, so this imagery should be able to satisfy intelligence tasks for NIIRS levels 3 and 4. Although the highest NIIRS and EEI values were obtained with the TIFF products, the level of processing was not found to be a significant predictor of NIIRS in the sample size used. As might be expected, GSD was found to be significant predictor of NIIRS for both formats. The range in average NIIRS values for the entire sample of TIFF and GeoTIFF images was 3.61 to 5.28, with NIIRS values increasing as collected GSD decreased. A statistical analysis shows that the IQE for two formats had statistically different slopes. It is suspected that a broken-line IQE is more appropriate for the GeoTIFF images, but such a model could not be distinguished from a single linear equation with the data available. Because TIFF images are higher NIIRS than GeoTIFF images when the collected GSD is actually less than one meter, the TIFF image format is recommended for intelligence EEI-type application if the user has the option. This study indicates that IKONOS panchromatic products can satisfy requirements for NIIRS level 4 imagery. Where the best possible satisfaction of image tasks is required, the highest collected resolution (i.e., at nadir) IKONOS panchromatic imagery should be acquired. For imagery where coordinate embedded pixels are not required (as in GeoTIFF) and submeter GSD is assured, TIFF products should be obtained.

For imagery where coordinate embedded pixels are not required (as in GeoTIFF) and submeter GSD is assured, TIFF products should be obtained.

7. Conclusions and summary

Several different types of Space Imaging IKONOS products were evaluated for their spatial resolution. Overall the image quality has been excellent and as advertised, but the variety of options was new to many of the scientists using the data. The spatial resolution was also relatively stable over the period of the work. The wide variety of products available from Space Imaging and the lack of access to raw imagery also makes comparison with system-level specifications difficult. First, the product is compressed onboard the spacecraft. Although little degradation in the imagery is noticeable, classic linear system analysis definitions do not necessarily hold. Second, the imagery is processed with several proprietary algorithms. The georeferenced imagery is also resampled with two different kernels: cubic convolution and nearest neighbor. MTFC processing, when performed, is integrated with the various resampling methods, which is a new paradigm for the government that historically has had extensive oversight of the construction of remote sensing systems. For these systems, product characterization needs to be considered instead of system characterization.

MTFC processing improves imagery quality but increases noise. The panchromatic imagery noise level is increased by over a factor of 4. Although not many truly dark targets have been available for examination, imaging over water bodies, forest, and other dark targets without MTFC is probably the best option. Native GSD imagery has better interpretability than resampled imagery; however, NIMA is presently the only government agency that can obtain this product.

Comparing results between different groups is challenging because all groups did not evaluate the same products. A more intuitive approach is to follow the GIQE, in which

edge response, GSD, SNR, and processing methods are used to define the spatial resolution requirements in terms of the MTF at the Nyquist frequency. Although the GIQE has not been fully tested for the various IKONOS product options, developing specifications in terms of the GIQE parameters could be beneficial.

Currently it is very difficult to measure MTF at high spatial frequencies on-orbit because the SNR of such measurements degrades with increasing spatial frequency. Because these measurements are often noisy and difficult to interpret, other simpler and more intuitive metrics, such as the width of the Point Spread Function, the Line Spread Function, or the slope of the edge response, may be more practical and useful. These three characteristics are all related by Fourier transforms, so measuring any one characteristic allows determination of the other two.

Acknowledgments

This work was supported by the NASA Earth Science Applications Directorate under contract number NAS 13-650 at the John C. Stennis Space Center, Mississippi.

References

Castleman, Kenneth R. (1996). *Digital Image Processing*. (pp. 667). Upper Saddle River, New Jersey: Prentice Hall.

Civil NIIRS Reference Guide (1996). Imagery Resolution Assessment and Reporting Standards Committee. http://www.fas.org/irp/imint/niirs_c/guide.htm, accessed June 12, 2003.

Garvin, J.B., Mahmood, A., & Yates, J. (2002). Monitoring landscapes on oceanic islands: sub-meter imaging from IKONOS in the context of RADARSAT SAR. *Proceedings of the 2002 High Spatial Resolution Commercial Imagery Workshop*, March 25-27, Reston, VA, USA, sponsored by NASA/NIMA/USGS Joint Agency Commercial Imagery Evaluation Team. CD-ROM.

General Image Quality Equation (GIQE) User's Guide, Version 4.0 (1996). National Imagery and Mapping Agency.

Holst, G.C., (1995). *Electro-Optical Imaging System Performance*. (pp. 146-147). Bellingham, Washington: SPIE Optical Engineering Press.

Leachtenauer, J.C., Malila, W., Irvine, J.M., Colburn, L.P., and Salvaggio, N.L. (1997). General Image-Quality Equation: GIQE. *Applied Optics*, 36 (32), 8322-8328.

Pagnutti, M., Ryan, R., Kelly, M., Holekamp, K., Zanoni, V., Thome, K., & Schiller, S. (2003) Radiometric characterization of IKONOS multispectral imagery. *Remote Sensing of Environment, (this issue)*.

Rauchmiller, Robert F. and Schowengerdt, Robert A. (1988). Measurement of the Landsat Thematic Mapper MTF Using an Array of Point Sources. *Optical Engineering*, 27(4), 334 – 343.

Reichenbach, S. E., Park, S. K., and Narayanswamy, R. (1991), Characterizing digital image acquisition devices. *Optical Engineering*, 30, 170-177.

Schowengerdt, R. A. (1997). *Remote Sensing – Models and Methods for Image Processing*. (pp. 522). San Diego, California: Academic Press.

Schowengerdt, R. A., Archwamety, C. & Wrigley, R.C. (1985). Landsat Thematic Mapper Image - Derived MTF. *Photogrammetric Engineering and Remote Sensing*, 51(9), 1395 – 1406.

Storey, James C. (2001). Landsat 7 on-orbit modulation transfer function estimation. In H. Fujisada, J.B. Lurie, & K. Weber (Eds.), *Sensors, Systems, and Next-Generation Satellites V: Proceedings of SPIE, 4540*, 50-61,

Tucker, Dr. Compton J. (2002). From Agamemnon to IKONOS – in search of the Trojan War. *Proceedings of the 2002 High Spatial Resolution Commercial Imagery Workshop*, March 25-27, Reston, VA, USA, sponsored by NASA/NIMA/USGS Joint Agency Commercial Imagery Evaluation Team. CD-ROM.

Tzannes, A. P., and Mooney, J. M. (1995). Measurement of the modulation transfer function of infrared cameras, *Optical Engineering*, 34, 1808-1817.

Vitae

Insert vitae here.

Figure Legends

Fig. 1. Big Spring target (August 5, 2001) with MTFC-off (left) and with MTFC-on (right). The Roberts gradient magnitude images are shown directly below. Note the sharper gradient in the MTFC-on case. The amplitude of the gradient is greater in the latter case.

Fig. 2. Illustration of tarp orientation with respect to true north and corresponding example image.

Fig. 3. Edge spread function projection from angled ground sample interval points.

Fig. 4. A blurred edge and differentiation of the edge to locate the point of maximum slope.

Fig. 5. IKONOS multispectral image of blue tarps deployed at Brookings, South Dakota, on July 25, 2001.

Fig. 6. Pulse response function obtained from blue tarps on July 25, 2001.

Fig. 7. Input pulse function and output pulse response.

Fig. 8. Input sinc function and output response in Fourier space.

Fig. 9. MTF function for the blue tarp target on July 25, 2001.

Fig. 10. Overplot of four estimates of blue band pulse response functions from blue tarps.

Fig. 11. Overplot of four estimates of blue band MTF functions from blue tarps.

Fig. 12. IKONOS panchromatic images of the edge target tarps deployed at Stennis Space Center, Mississippi, for the easting direction measurement on January 15, 2002, (left) and for the northing direction measurement on February 17, 2002 (right). Gray rectangular frames overlaid on the tarp images show the areas selected for the edge response analyses.

Fig. 13. Measured edge responses (left column) and the best fits to them with superposition of three sigmoidal functions (right column). Data are for the measurements in the northing direction using the IKONOS image acquired on February 17, 2002, and processed either with MTFC-on (bottom row) or with MTFC-off (top row). Respective image areas are shown on the left side of the figure.

Fig. 14. Superimposed edge responses and the fitted sigmoidal functions for the IKONOS images processed either with MTFC-on (bottom row) or MTFC-off (top row). Northing direction is the left column and easting direction is the right column.

Fig. 15. Line spread functions derived from the fitted edge responses for the IKONOS images processed either with MTFC-on (bottom row) or with MTFC-off (top row). Northing direction is the left column and easting direction is the right column.

Tables

Table 1

Noise gain associated with MTFC processing

Band	Noise Gain
Blue	1.59
Green	1.63
Red	1.68
NIR	1.81
Pan	4.16

Table 2

Reference image comparisons for sharpness quality metric

Location	Processing	Average DN gradient	Average percent difference
Big Spring, Texas	MTFC-off	54.2	44.3
	MTFC-on	78.2	
Tucson, Arizona	MTFC-off	60.97	31.8
	MTFC-on	80.38	

Table 3

Anniversary image pair solar and sensor angles

Date	Solar azimuth (°)	Solar elevation (°)	Sensor azimuth (°)	Sensor elevation (°)
July 23, 2000	113.8	65.4	136.1	84.2
July 15, 2001	117.7	70.2	276.8	84.1

Table 4

Average DN gradient magnitudes for Tucson sites

Date	Area 1 (residential) 499x406 pixels	Area 2 (road/industrial) 424x451 pixels
July 23, 2000	167.2	129.7
July 15, 2001	159.5	118.1

Table 5

Line spread function FWHM for IKONOS panchromatic images (Jan/Feb 2002)

	Easting (m)	Northing (m)
MTFC-off	1.45	1.27
MTFC-on	0.85	0.52

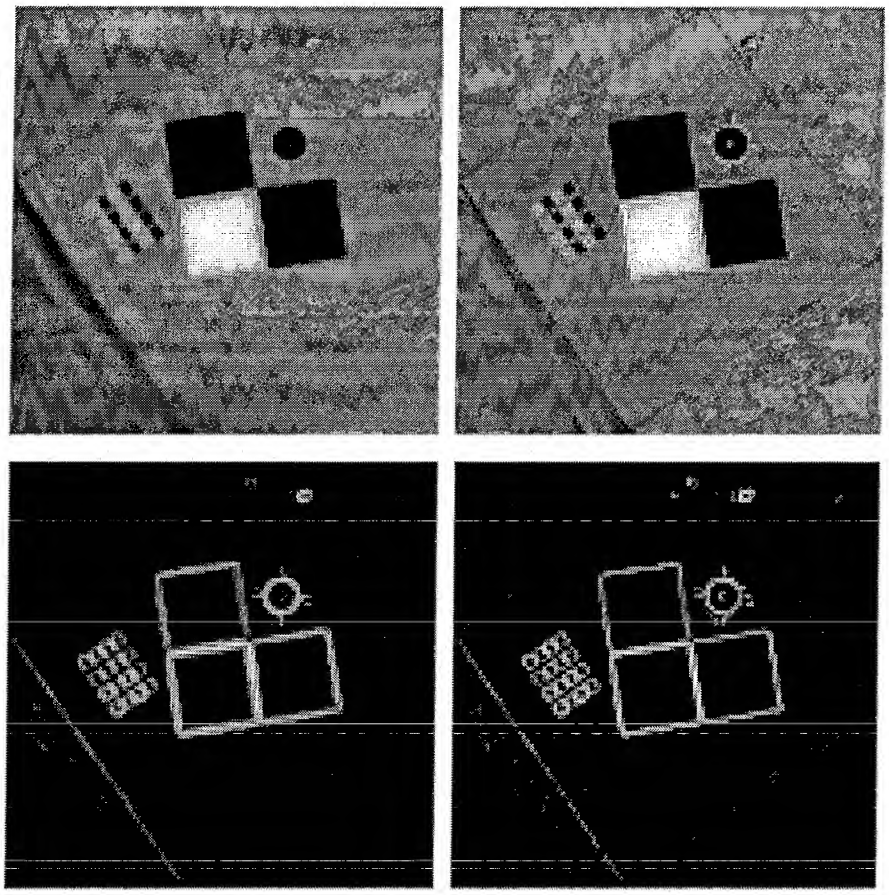

Fig. 1. Big Spring target (August 5, 2001) with MTFC-off (left) and with MTFC-on (right). The Roberts gradient magnitude images are shown directly below. Note the sharper gradient in the MTFC-on case. The amplitude of the gradient is greater in the latter case.

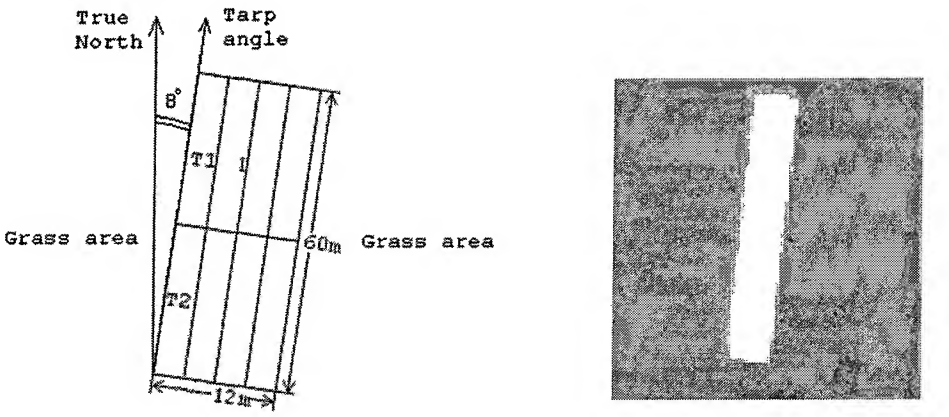

Fig. 2. Illustration of tarp orientation with respect to true north and corresponding example image.

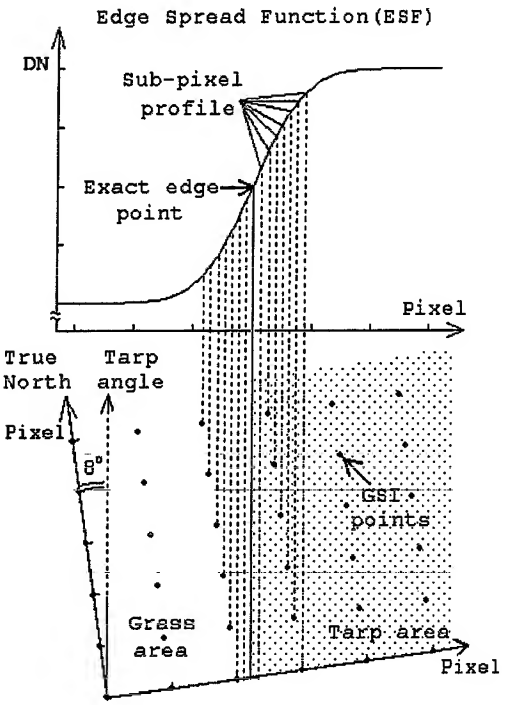

Fig. 3. Edge spread function projection from angled ground sample interval points.

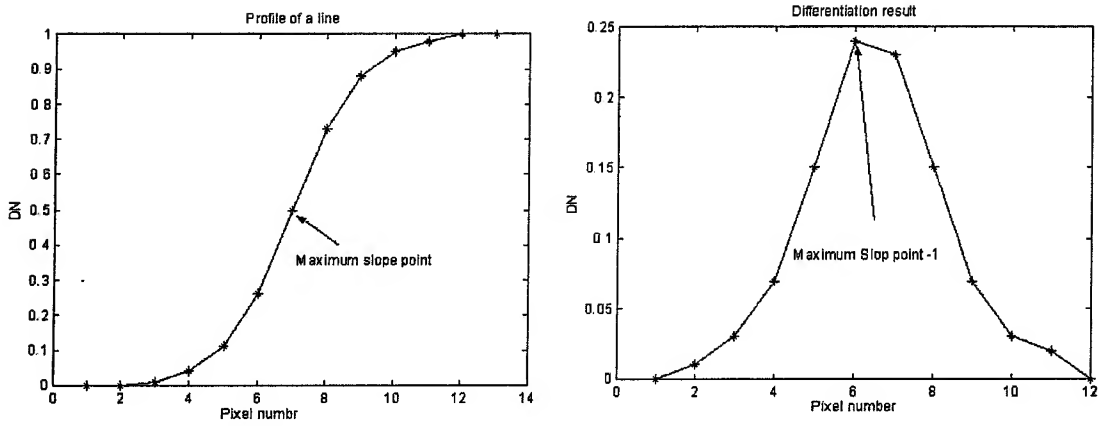

Fig. 4. A blurred edge and differentiation of the edge to locate the point of maximum slope.

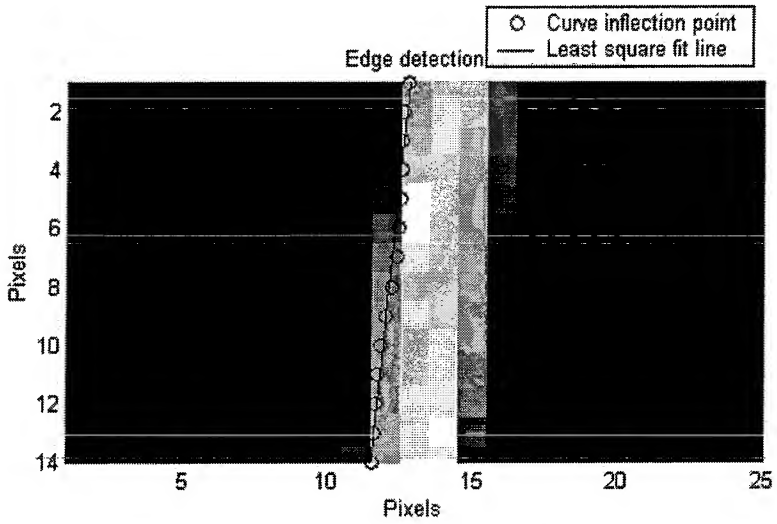

Fig. 5. IKONOS multispectral image of blue tarps deployed at Brookings, South Dakota, on July 25, 2001.

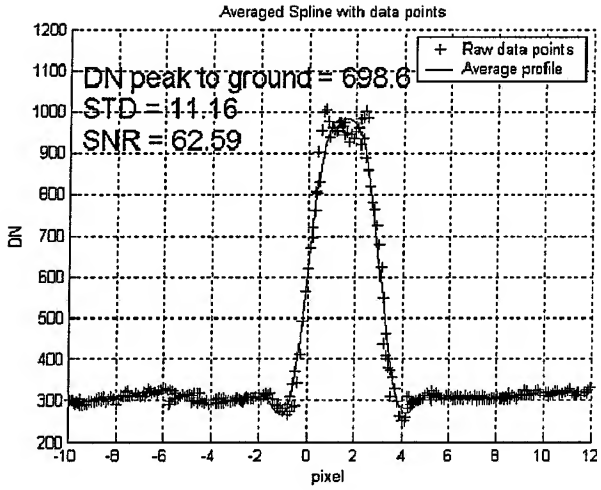

Fig. 6. Pulse response function obtained from blue tarps on July 25, 2001.

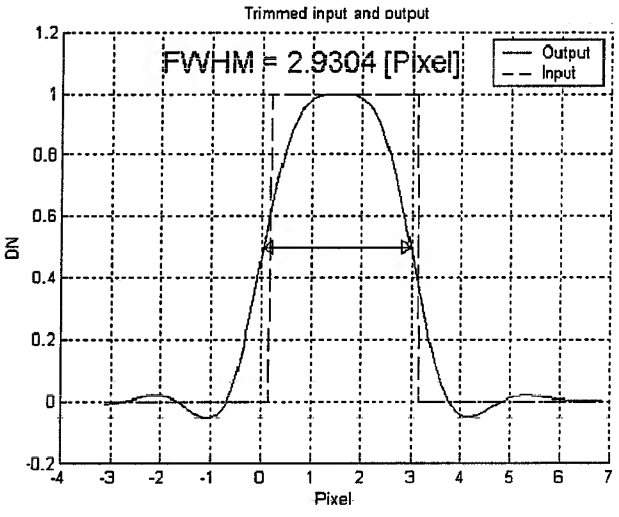

Fig. 7. Input pulse function and output pulse response.

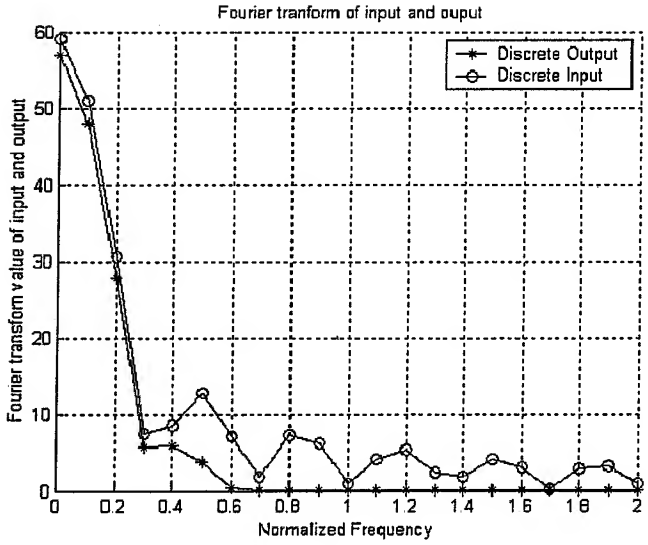

Fig. 8. Input sinc function and output response in Fourier space.

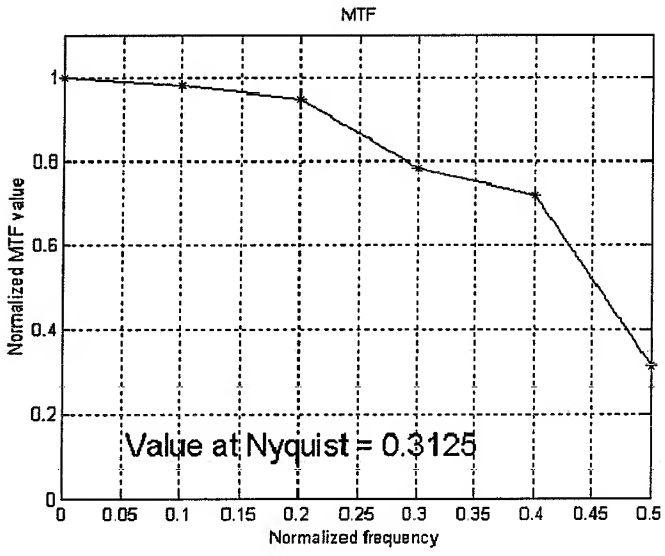

Fig. 9. MTF function for the blue tarp target on July 25, 2001.

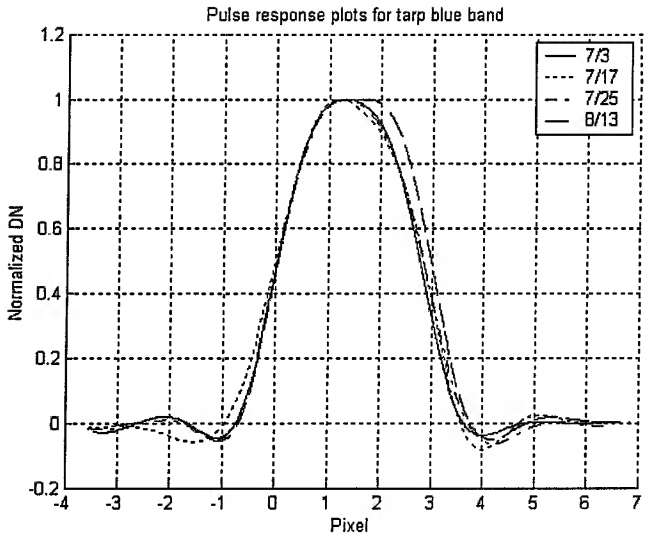

Fig. 10. Overplot of four estimates of blue band pulse response functions from blue tarps.

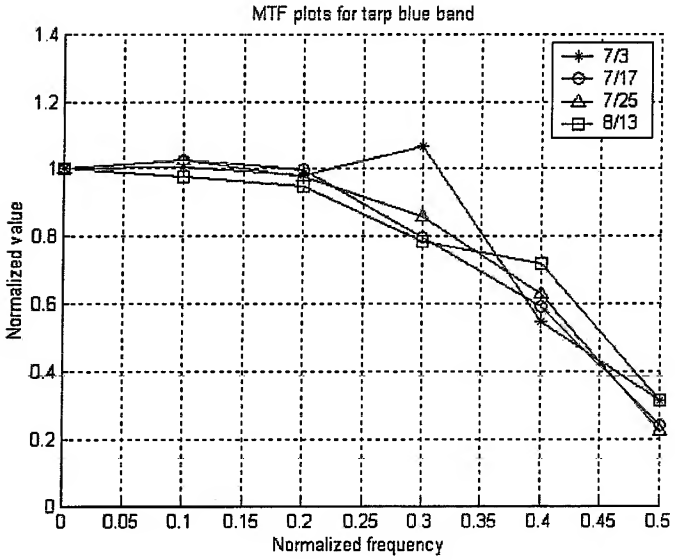

Fig. 11. Overplot of four estimates of blue band MTF functions from blue tarps.

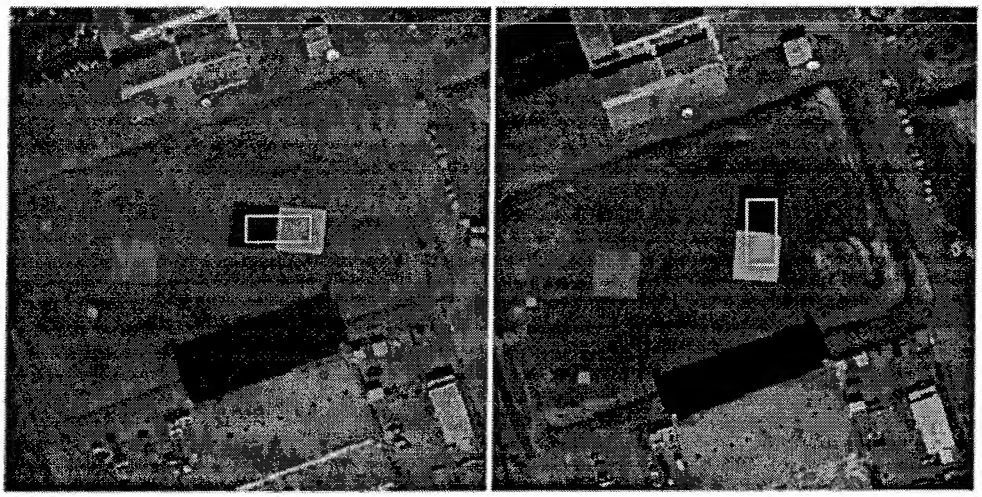

Fig. 12. IKONOS panchromatic images of the edge target tarps deployed at Stennis Space Center, Mississippi, for the easting direction measurement on January 15, 2002, (left) and for the northing direction measurement on February 17, 2002 (right). Gray rectangular frames overlaid on the tarp images show the areas selected for the edge response analyses.

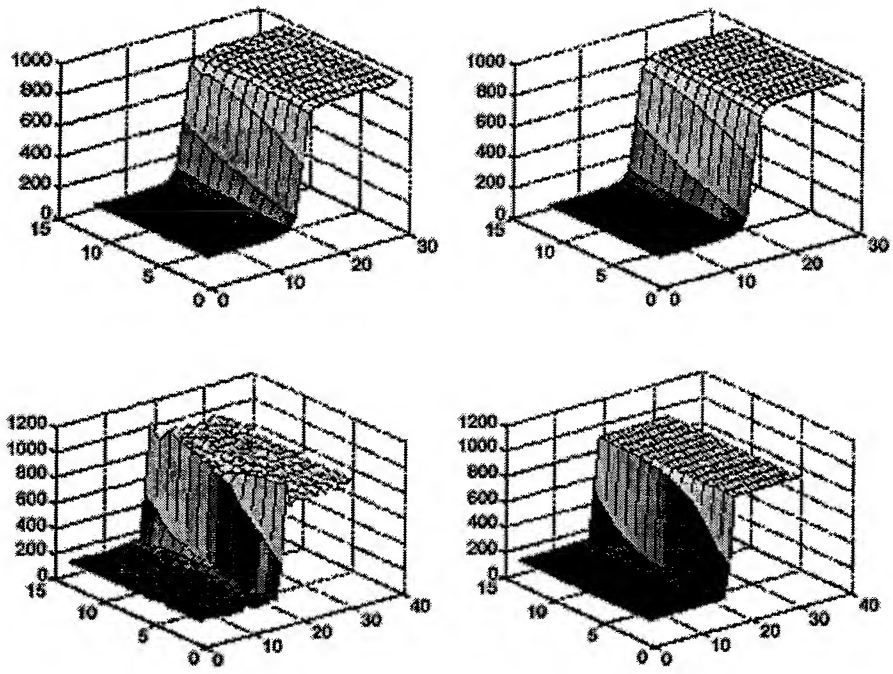

Fig. 13. Measured edge responses (left column) and the best fits to them with superposition of three sigmoidal functions (right column). Data are for the measurements in the northing direction using the IKONOS image acquired on February 17, 2002, and processed either with MTFC-on (bottom row) or with MTFC-off (top row). Respective image areas are shown on the left side of the figure.

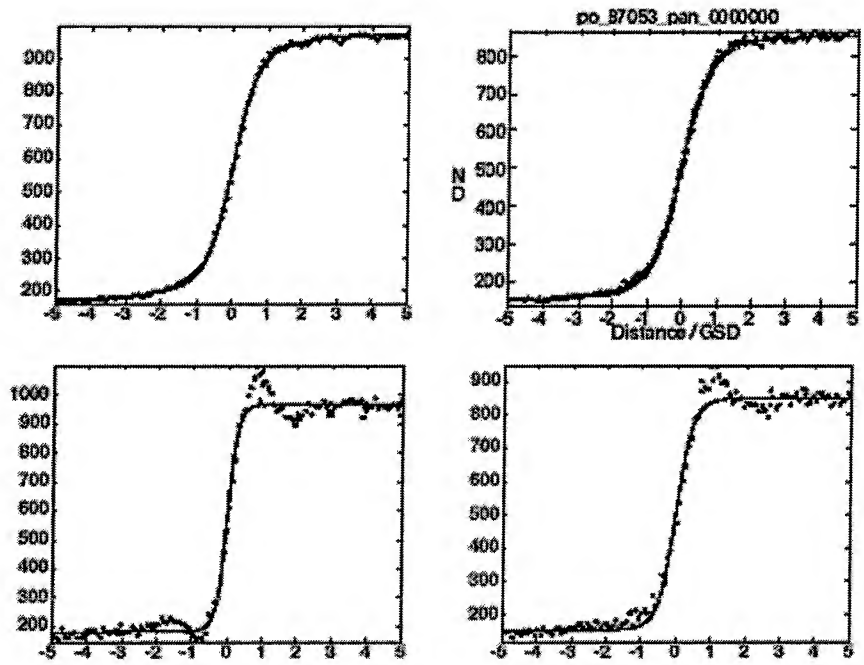

Fig. 14. Superimposed edge responses and the fitted sigmoidal functions for the IKONOS images processed either with MTFC-on (bottom row) or MTFC-off (top row). Northing direction is the left column and easting direction is the right column.

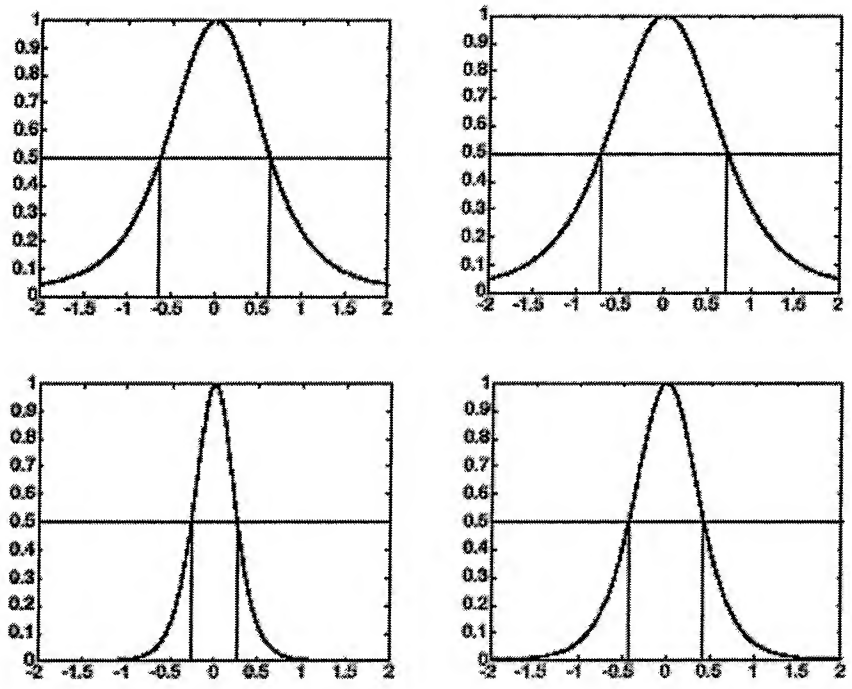

Fig. 15. Line spread functions derived from the fitted edge responses for the IKONOS images processed either with MTFC-on (bottom row) or with MTFC-off (top row). Northing direction is the left column and easting direction is the right column.

REPORT DOCUMENTATION PAGE

Form Approved
OMB No. 0704-0188

1. REPORT DATE *(DD-MM-YYYY)*	2. REPORT TYPE	3. DATES COVERED *(From - To)*
29-05-2003		

4. TITLE AND SUBTITLE
IKONOS Spatial Resolution and Image Interpretability Characterization

5a. CONTRACT NUMBER

5b. GRANT NUMBER

5c. PROGRAM ELEMENT NUMBER

6. AUTHOR(S)
Robert Ryan
Braxton Baldridge
Robert Schowengerdt
Taeyoung Choi
Dennis Helder
Slawomir Blonski

5d. PROJECT NUMBER

5e. TASK NUMBER

5f. WORK UNIT NUMBER

7. PERFORMING ORGANIZATION NAME(S) AND ADDRESS(ES)
LMSO

8. PERFORMING ORGANIZATION REPORT NUMBER
SE-2003-05-00042-SSC

9. SPONSORING/MONITORING AGENCY NAME(S) AND ADDRESS(ES)
Earth Science Directorate

10. SPONSORING/MONITOR'S ACRONYM(S)

11. SPONSORING/MONITORING REPORT NUMBER

12. DISTRIBUTION/AVAILABILITY STATEMENT
Publicly Available STI per form 1676

13. SUPPLEMENTARY NOTES
Journal Name Remote Sensing of Environment

14. ABSTRACT

15. SUBJECT TERMS

16. SECURITY CLASSIFICATION OF:			17. LIMITATION OF ABSTRACT	18. NUMBER OF PAGES	19b. NAME OF RESPONSIBLE PERSON
a. REPORT	b. ABSTRACT	c. THIS PAGE			Robert Ryan
U	U	U	UU	49	19b. TELEPHONE NUMBER *(Include area code)* (228) 688-1868